Electronic Supplementary Material (ESI) for Physical Chemistry Chemical Physics.

Supporting Information

Dimensionality reduction induced synergetic optimization of the thermoelectric properties in $Bi_2Si_2X_6$ (X=Se, Te) monolayers

Tingting Zhang[a], Suiting Ning[a], Ziye Zhang[a], Ning Qi[a], and Zhiquan Chen*[a]

[a]*Hubei Nuclear Solid Physics Key Laboratory, Department of Physics,*

Wuhan University, Wuhan 430072, China

* E-mail: chenzq@whu.edu.cn

Table S1: The optimized lattice constants of bulk $Bi_2Si_2Te_6$.

		PBE	PBEsol	D2	D3	experiment
$Bi_2Si_2Te_6$	a (Å)	7.380	7.280	7.216	7.345	7.270
	c (Å)	23.594	21.243	21.591	21.738	21.343

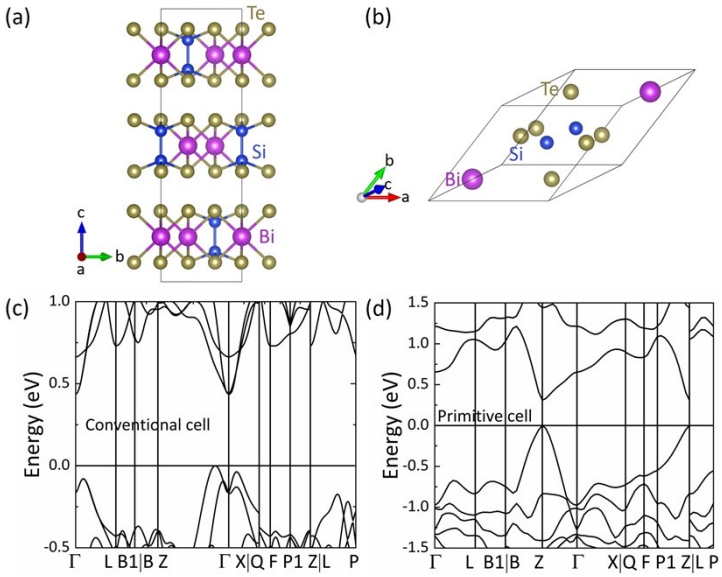

Figure S1. (a) Conventional and (b) primitive cell structures of $Bi_2Si_2Te_6$, and band structure of $Bi_2Si_2Te_6$ with (c) conventional cell structure and (d) primitive cell structure.

Table S2: The elastic constants of bulk and monolayer $Bi_2Si_2X_6$ (X=Se, Te) (unit: GPa).

		C11 (C22)	C12	C13 (C23)	C33	C44 (C55)	C66
$Bi_2Si_2Se_6$	Bulk	69.75	26.28	8.18	16.73	5.21	21.73
	ML	19.00	7.09	0.28	0.50	0.88	6.03
$Bi_2Si_2Te_6$	Bulk	55.05	17.19	10.01	19.06	9.81	18.93
	ML	15.33	4.50	-0.07	0.01	0.20	5.25

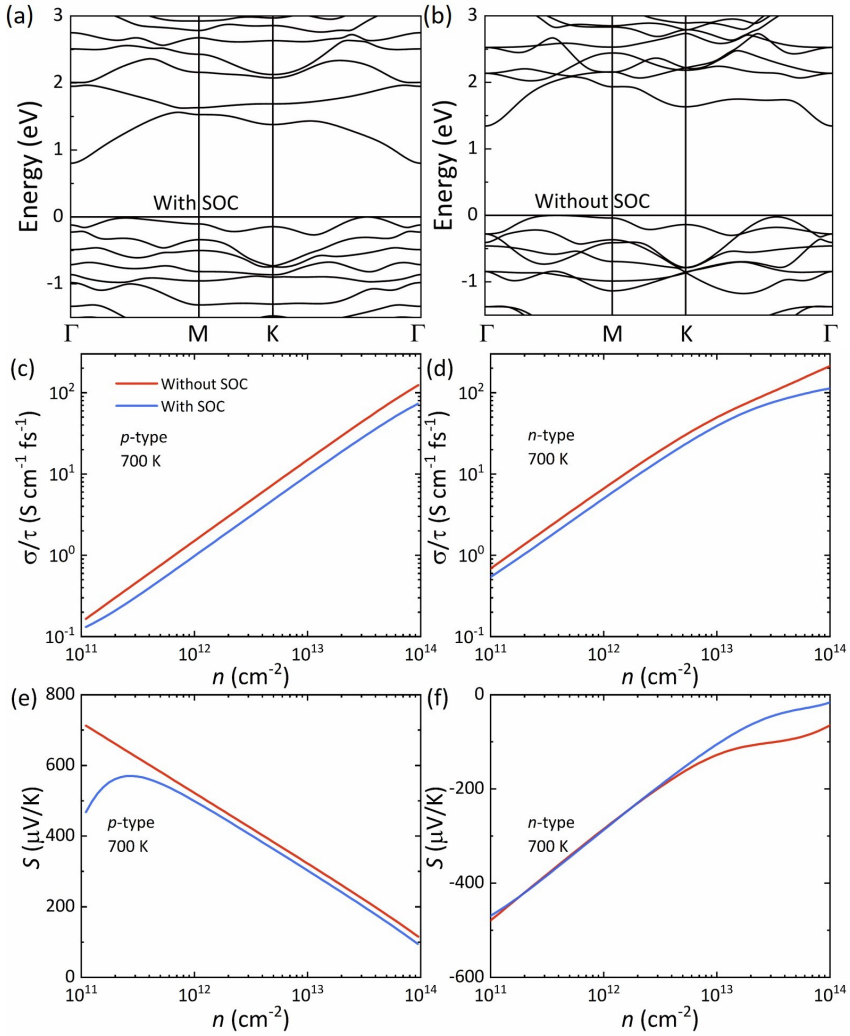

Figure S2: The calculated band structures of monolayer $Bi_2Si_2Te_6$ (a) with SOC and (b) without SOC, ratio of electrical conductivity to carrier relaxation time and Seebeck coefficient for (c and e) p-type and (d and f) n-type monolayer $Bi_2Si_2Te_6$ at 700 K.

The effect of SOC on electronic structure and electronic properties:

In Figure S2 (a) and (b), the calculated band gaps of monolayer $Bi_2Si_2Te_6$ with and without SOC are 0.80 and 1.34 eV, respectively. For the p-type monolayer $Bi_2Si_2Te_6$, ratio of electrical conductivity to carrier relaxation time σ/τ and Seebeck coefficient S without SOC effect are larger than that with SOC, which will overestimate its TE performance. For the n-type monolayer $Bi_2Si_2Te_6$ without SOC, σ/τ is also higher, while S is almost consistent at low concentration and has a difference at high concentration.

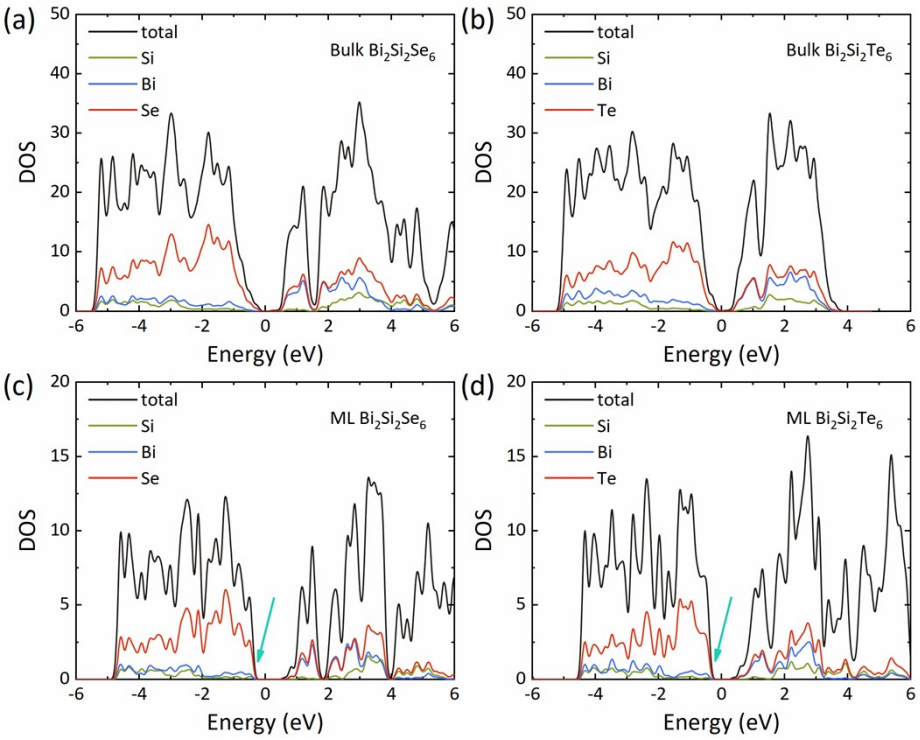

Figure S3: The density of states (DOS) of (a) bulk $Bi_2Si_2Se_6$, (b) bulk $Bi_2Si_2Te_6$, (c) monolayer $Bi_2Si_2Se_6$ and (d) monolayer $Bi_2Si_2Te_6$.

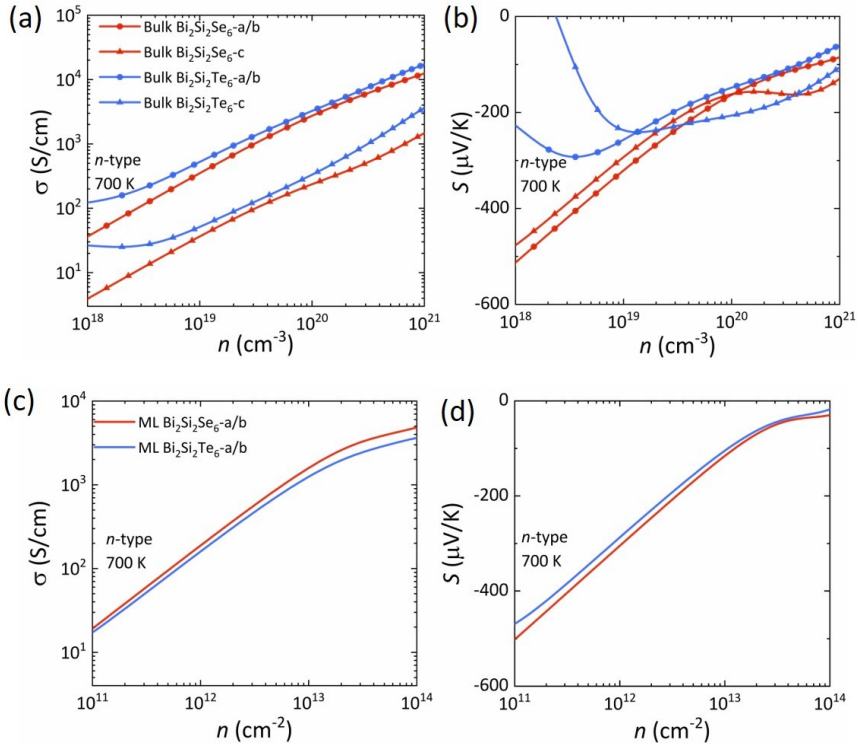

Figure S4: The (a and c) electrical conductivity and (b and d) Seebeck coefficient for the n-type bulk and monolayer $Bi_2Si_2X_6$ at 700 K.

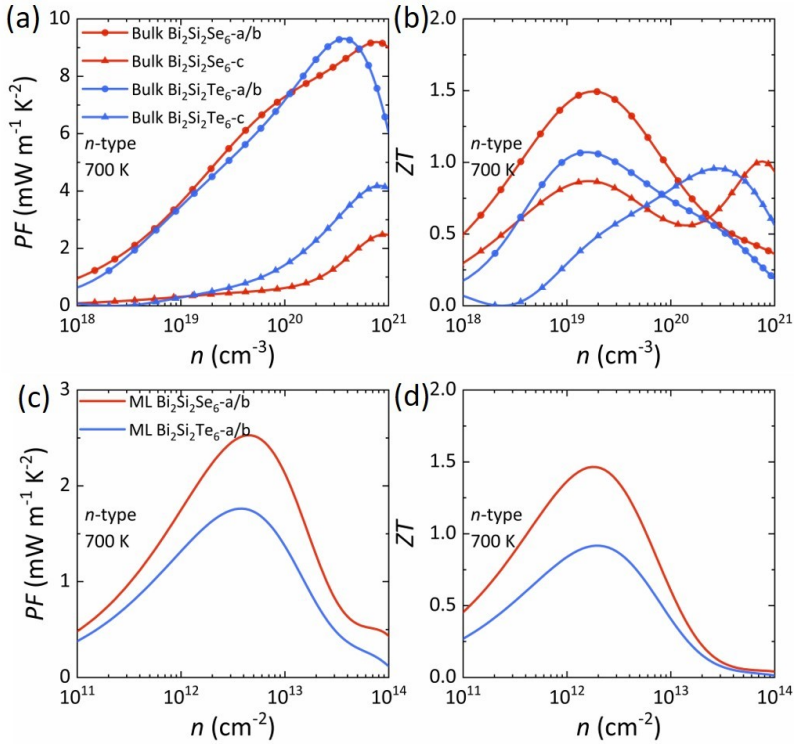

Figure S5: The (a and c) power factor and (b and d) dimensionless figure of merit for the n-type bulk and monolayer $Bi_2Si_2X_6$ at 700 K.

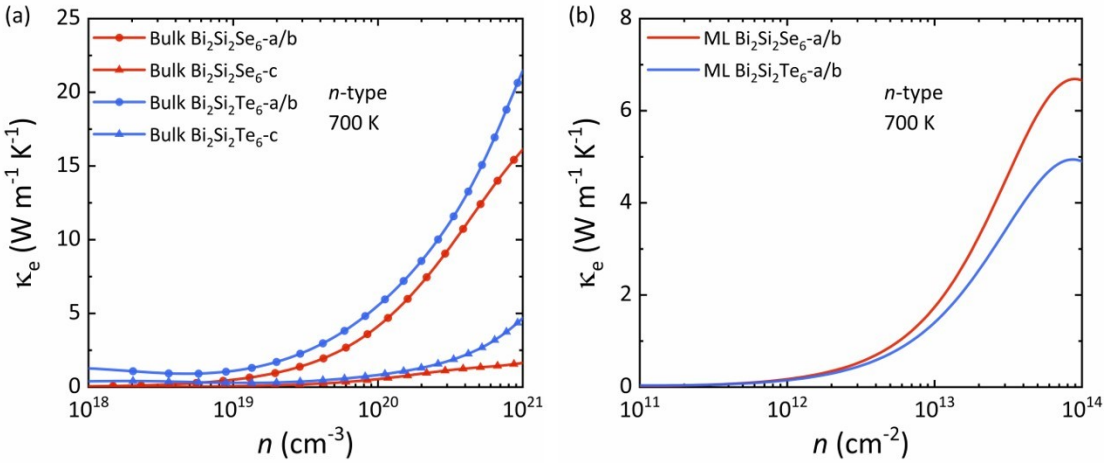

Figure S6: The electronic thermal conductivity of n-type (a) bulk and (b) monolayer $Bi_2Si_2X_6$ at 700 K.

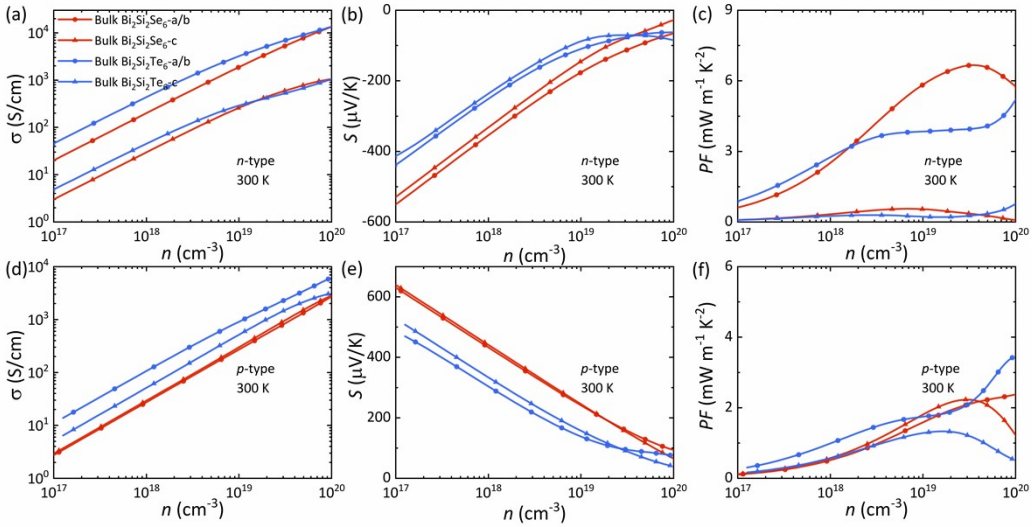

Figure S7: The (a and d) electrical conductivity, (b and e) Seebeck coefficient and (c and f) power factor for the n- and p-type bulk $Bi_2Si_2X_6$ at 300 K.

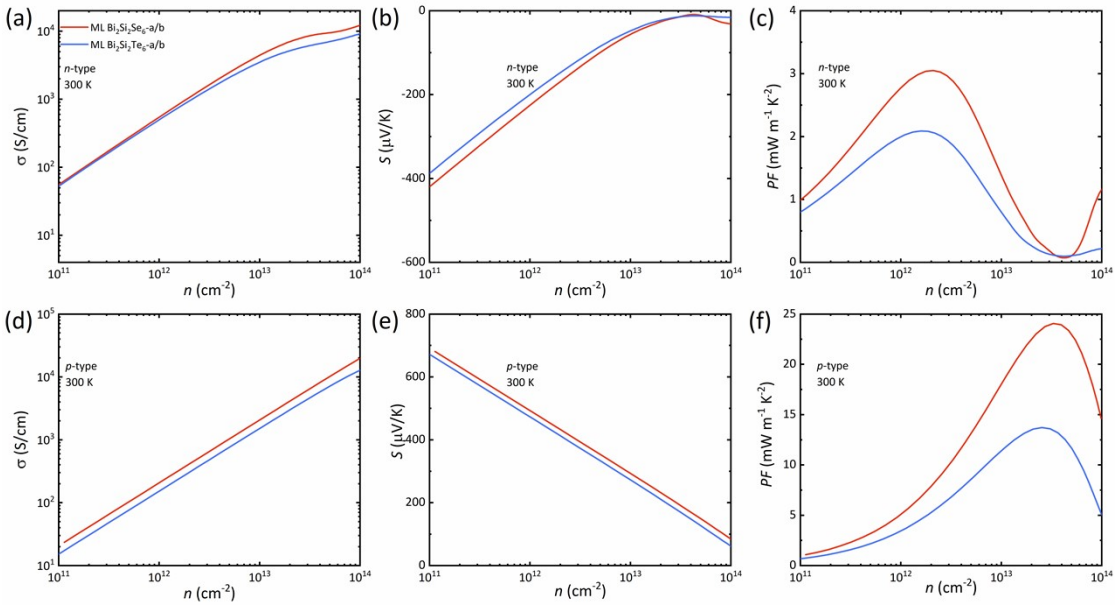

Figure S8: The (a and d) electrical conductivity, (b and e) Seebeck coefficient and (c and f) power factor for the n- and p-type monolayer $Bi_2Si_2X_6$ at 300 K.

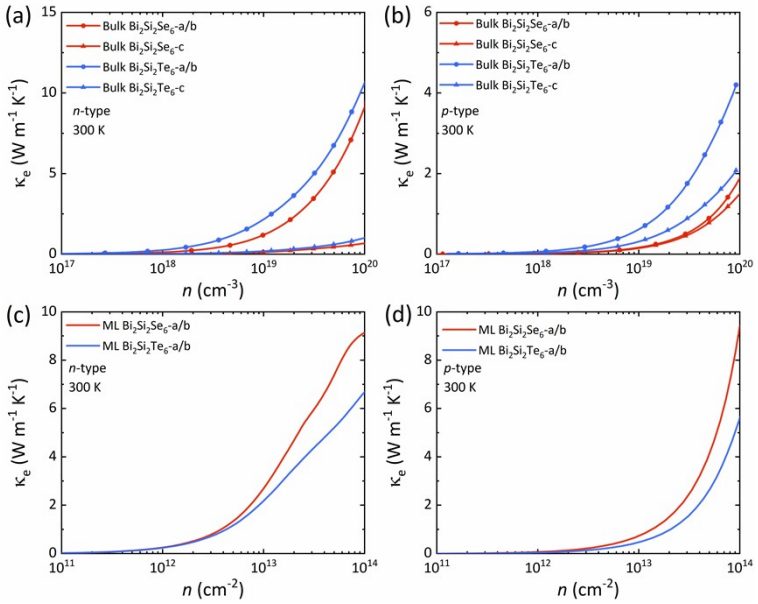

Figure S9: The electronic thermal conductivity of (a) n- and (b) p-type bulk, and (c) n- and (d) p-type monolayer $Bi_2Si_2X_6$ at 300 K.

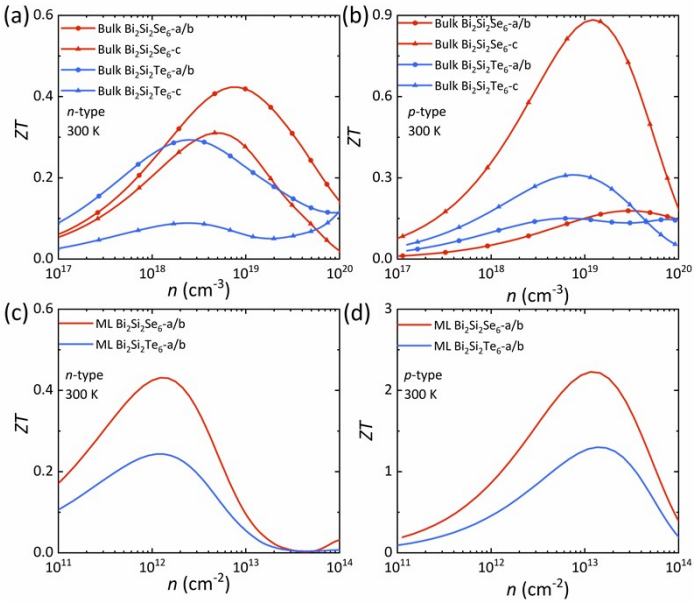

Figure S10: The dimensionless figure of merit of (a) n- and (b) p-type bulk, and (c) n- and (d) p-type monolayer $Bi_2Si_2X_6$ at 300 K.

Table S3: The predicted Debye temperature ($^{\theta_D}$:K), phonon group velocities (km s^{-1}) in each mode (υ_l for longitudinal acoustic phonon mode, υ_t for transverse acoustic phonon mode), and average phonon group velocity υ_m (km s^{-1}) of bulk and monolayer $Bi_2Si_2X_6$ (X=Se, Te).

		θ_D	v_l	v_t	v_m
$Bi_2Si_2Se_6$	Bulk	151.2	2.48	1.37	1.53
	ML	84.8	1.97	1.18	1.31
$Bi_2Si_2Te_6$	Bulk	142.2	2.37	1.37	1.52
	ML	61.0	1.50	0.89	0.99